CrossMark
click for updates

View Article Online
View Journal

PCCP

Accepted Manuscript

This article can be cited before page numbers have been issued, to do this please use: X. Song, Y. Liu, Y. Zhang, K. Ding, S. Nie and P. Yang, *Phys. Chem. Chem. Phys.*, 2016, DOI: 10.1039/C5CP07187A.

This is an *Accepted Manuscript*, which has been through the Royal Society of Chemistry peer review process and has been accepted for publication.

Accepted Manuscripts are published online shortly after acceptance, before technical editing, formatting and proof reading. Using this free service, authors can make their results available to the community, in citable form, before we publish the edited article. We will replace this *Accepted Manuscript* with the edited and formatted *Advance Article* as soon as it is available.

You can find more information about *Accepted Manuscripts* in the Information for Authors.

Please note that technical editing may introduce minor changes to the text and/or graphics, which may alter content. The journal's standard Terms & Conditions and the Ethical guidelines still apply. In no event shall the Royal Society of Chemistry be held responsible for any errors or omissions in this *Accepted Manuscript* or any consequences arising from the use of any information it contains.

ROYAL SOCIETY OF CHEMISTRY

www.rsc.org/pccp

View Article Online
DOI: 10.1039/C5CP07187A

Physical Chemistry Chemical Physics

ARTICLE

Synthesis of butterfly-like ZnO and their reducing ability for Au^{3+} ions towards enhanced photocatalysis

Received 00th January 20xx,
Accepted 00th January 20xx

DOI: 10.1039/x0xx00000x

www.rsc.org/

Xueling Song, Yumeng Liu, Yan Zheng, Kun Ding, Shijie Nie, and Ping Yang*

Zinc oxide (ZnO) with diverse morphologies have been successfully fabricated through a simple one-step hydrothermal synthesis and subsquent calcined treatment. The formation of butterfly-like ZnO is mainly ascribed to a typical nucleation-growth-assembly process because of the electrostatic interactions between nanoparticles and the reconstruction of sheets. Without using any reducing agents, Au nanoparticles (NPs) created from Au^{3+} ions were deposited on the butterfly-like ZnO with simply stirring at room temperature. It was found that tartaric acid was existed in ZnO calcined at low temperature (300 °C) resulted in ZnO with reducing ability for Au^{3+} ions. The Au NPs connected closely with ZnO matrix. Such colsed connection results in the hierarchical ZnO-Au composites with efficient photocatalytic activity for environmental remediation. Compared with pure ZnO sample calcined at 300 °C, the hierarchical ZnO-Au composite exhibited enhanced photocatalytic performance for Rhodamine B. Photodegradation results indicated that the incorporation of Au nanoparticles drastically increased photocatalytic efficiency by promoting the separation process of the electron–hole pairs created by the absorption of photon.

Introduction

Recently, metal oxide semiconductor materials with various morphologies have been stimulated remarkable attention because of their unique physical and chemical properties, which make them widely applied in many fields, such as photocatalysts, gas sensors, lithium ion batteries.[1-5] Among metal oxide materials, zinc oxide (ZnO), as an important category of direct wide-band gap semiconductor, has aroused a great deal of interest due to its broaden applications, i.e., photocatalytic degradation of organic pollutants, detecting toxic and deleterious gases, and even used in monitoring human health.[6, 7] Hierarchical structure 3-dimentional (3D) materials created from the self-assembly of 1D or 2D building blocks, in particular, have exhibited unique optical and electrical properties which are different from those of mono-morphological structures.[7,8] Previous studies have demonstrated that ZnO was easily constructed into various morphologies from nanoparticles (NPs),[9, 10] nanorods, nanowires,[11] and nanosheets[6, 12]. To the best of our own knowledge, the performances of ZnO materials were greatly depended on their microstructure, composition and surface modification.[6, 13, 14] Therefore, it is indispensable to synthesize 3D ZnO with hierarchical structure.

It is well known that the synthesis of 3D hierarchical ZnO is closely associated with shape-directing/capping agents, such as polyvinyl pyrrolidone (PVP), hexadecyltrimethylammonium bromide (CTAB), ascorbate ion and so on. Furthermore, Wang and co-workers synthesized 3D nest-like ZnO with hierarchically porous structures by using PVP as a morphology-controlling agent exhibiting excellent gas sensing performance toward ethonal.[15] Raula and co-workers obtained hierarchical flower-like ZnO by applying ascorbate ion as a shape-directing agent showing high catalytic activity.[16] However, tartaric acid (TA) as an extremely successful modifier molecule is not widely used in prepare hierarchical ZnO. Yang and co-workers have prepared rod-like ZnO mesocrystals using TA as the additive showing decent photocatalytic performance.[17] Thus, the synthesis of hierarchical ZnO by applying TA as surfactant is still a new challenge.

Owing to the relatively low charge separation efficiency and fast the recombination of photon-generated carriers under UV irradiation, the pure ZnO material reveals low photoenergy conversion efficiency.[3, 18] Thus, many methods have been attempted to inhibit the charge recombination by forming composite between semiconductors and electron scavenging agents (i.e., noble metals, metal sulfide, carbon nitride materials)[19-20]. Thereinto, it has been reported that incorporating Au NPs on the surface of ZnO has been regarded as one of the most effective methods because the performance of ZnO can be greatly enhanced not only in photocatalysis property but also in gas sensing performence.[22] Up to now, there are many practical procedures to introduce noble metals (e.g., Au, Ag, and Pt) onto semiconductors, such as chemical approaches, thermal strategies, sputtering

[a] School of Material Science and Engineering, University of Jinan, Jinan, 250022, P.R. China, Fax: +86-531-87974453; Tel: +86-531-89736225; Email: mse_yangp@ujn.edu.cn.

†Electronic Supplementary Information (ESI) available: XRD patterns of the precursor, ZnO synthesized at 150 °C and ZnO-Au, and SEM images of ZnO products obtained by applying HMT as the alkali source at different reaction temperature. See DOI: 10.1039/x0xx00000x

Published on 12 January 2016. Downloaded by Michigan State University on 20/01/2016 01:18:50.

Physical Chemistry Chemical Physics Accepted Manuscript

View Article Online
DOI: 10.1039/C5CP07187A

Published on 12 January 2016. Downloaded by Michigan State University on 20/01/2016 01:18:50.

methods and photo-deposition routes.[23] For instance, Fageria and co-workers reported the synthesis of ZnO/Au heterostructure nanoflower using hydrazine hydrate as reducing agent and their application in photocatalysis under UV and visiblelight.[14] Moreover, they also demonstrated the formation of Fermi level equilibration between semiconductors and noble metals. Same group obtained ZnO/Au hybrid nanostructures by irradiating ZnO suspension containing $HAuCl_4$ with a 450 W Xenon lamp and reported their promoting photocatalytic activity and antibacterial activity.[3] Sung and co-workers reported that Au–ZnO composite photocatalysts were obtained by a sputtering method, which exhibit the enhanced photocatalyticactivity.[24] In addition, Manna and co-workers obtained hybrid Au/ZnO nanoparticles showing enhanced photocatalytic properties by a one-pot microwave-based method using $KAu(SCN)_4$ as a precursor which has been reported to synthesize various Au nanostructures in the recent studies.[25-27] However, there still are many disadvantages existed in the above-mentioned synthesis routes, such as high cost, energy consumption, and complex process. It is still retained a room to improve the photocatalysis performance of these composites. Therefore, it is still a challenge to find a facile route to design and engineer Au-ZnO nanostructures to enhance the photocatalytic efficiency.

Herein, we synthesized hierarchical butterfly-like ZnO through a hydrothermal method and a subsequent calcining process using TA as a surfactant. ZnO-Au composite was readily obtained by a simple stirring process at room temperature. It is worth mentioning that $HAuCl_4{\cdot}3H_2O$ can be easily reduced to Au NPs in the ZnO suspension without any adscititious reductants, indicating the self-reducing ability of ZnO obtained in our experiment. The formation mechanism of ZnO-Au composite was investigated on the basis of X-ray photoelectron spectroscopy (XPS) spectra and X-ray diffraction (XRD) measurement. The enhanced photocatalytic degradation efficiency was observed in ZnO-Au composite compared with pure ZnO sample.

Experimental section

Chemicals

Zinc nitrate hexahydrate ($Zn(NO_3)_2{\cdot}6H_2O$, AR), potassium hydroxide (KOH, AR), hexamethylenetetramine (HMT, AR), TA($C_4H_6O_6$, AR), anhydrous ethanol were supplied by Shanghai Chemical Reagent Company and Tianjin Chemical Reagent Company. Deionized water (resistivity ~ 18 MΩ·cm) used in the preparation process was obtained from a Milli-Q synthesis system. All chemicals were used as received without further purification.

Synthesis of ZnO crystals

In a typical procedure, 0.7437 g of $Zn(NO_3)_2{\cdot}6H_2O$ and 0.1403 g of KOH in a molar ratio of 1 : 1 were dissolved in 50 mL of water with vigorously magnetic stirring for 30 min. Then, 0.075 g of TA was added to the solution with magnetic stirring.

Table 1 Preparation conditions of ZnO[a]

Sample	$Zn(NO_3)_2$(M)	Alkali (M)	Temperature (°C)
1	0.05	KOH 0.05	100
2	0.05	KOH 0.05	150
3	0.05	KOH 0.05	200
4	0.05	KOH 0.10	100
5	0.05	KOH 0.15	100
6	0.05	HMT 0.05	100
7	0.05	HMT 0.10	100
8	0.05	HMT 0.15	100
9	0.05	HMT 0.05	150
10	0.05	HMT 0.10	150
11	0.05	HMT 0.15	150

[a]0.01 M of TA was applied in the synthesis of ZnO. The calcination temperature and time were 300 °C and 2 h, respectively.

After that, the resulting white suspension was hydrothermally treated at 100 °C for 6 h in a 100 mL Teflonlined stainless autoclave. Upon the autoclave cooling down to room temperature naturally, the white powders were collected by centrifugation and washed with water and anhydrous ethanol for several times, and then dried at 60 °C for 10 h. Finally, the above obtained precursors were calcined at 300 °C for 2 h in a muffle furnace with heating rate of 5 °C min^{-1}. Furthermore, in order to compare with typical ZnO products, ZnO was prepared by calcination at higher temperature of 700 °C, which was denoted as ZnO-700. Similarly, other parallel experiments were carried out by changing the reaction temperature, the alkaline or the concentration of alkaline using the same hydrothermal method and calcining process. Detailed preparation conditions were summarized in Table 1. Moreover, to investigate the formation mechanism of the typical sample, time-dependent experiments were carried out by varying reaction time.

Synthesis of hierarchical ZnO-Au composite

The deposition of Au NPs on ZnO samples was carried out via a simple stirring process as follows. 0.2 mmol of as-synthesized ZnO powders (sample 1 and sample 2) was dispersed well in 20 mL of H_2O. After vigorously magnetic stirring for 6 h at room temperature, 50 μL of $HAuCl_4{\cdot}3H_2O$ aqueous solution (40 mM) was dropwise added into suspension with homogeneously dispersed ZnO samples. The color of the suspension was changed from white into purple. The purple precipitates were obtained by centrifugation and washed for several times with H_2O and anhydrous ethanol after stirring for 30 min. The obtained ZnO-Au composites were denoted as sample 1-Au and sample 2-Au, respectively. Finally, the products were dried at 60 °C for 6 h for further characterization.

Characterization

XRD patterns of as-obtained samples were obtained on an X-ray diffractometer (Bruker D8, Germany) with a Cu Kα

Physical Chemistry Chemical Physics Accepted Manuscript

This journal is © The Royal Society of Chemistry 20xx

View Article Online
DOI: 10.1039/C5CP07187A

Published on 12 January 2016. Downloaded by Michigan State University on 20/01/2016 01:18:50.

radiation source, and recorded with a 2θ range from 10° to 80°. A QUANTA FEG 250 field-emission scanning electron microscope (SEM) equipped with energy dispersive X-ray spectra (EDS) and a JEOL JEM 2010F transmission electron microscopy (TEM) were applied to characterize the detailed morphology and microstructure of samples. Fourier transform-infrared (FTIR) spectra of samples were obtained using a FTIR spectrometer (Thermo Electron, Nicolet 380, United States) in a frequency range of 4000-500 cm^{-1} with KBr as a reference sample. The UV-vis diffuse reflectance spectra (DRS) and absorption spectra were recorded on a Hitachi U-4100 spectrophotometer. Room-temperature photoluminescence (PL) spectra were measured by a Hitachi F-4600 PL spectrometer. The element valence state was determined by using a VG Micro Tech ESCA 3000 X-ray photoelectron spectrometer (XPS) using monochromatic Al Kα at a pressure of 1×10^{-9} mbar. Photocurrent measurements were examined by a standard three-electrode cell with a platinum wire as counter electrode, Ag/AgCl as reference electrode, and a working electrode (as-prepared samples) applying 50 mL of Na_2SO_4 aqueous solution (0.1 M) as electrolyte.

Photocatalytic degradation measurement

The photocatalytic degradation activities of pure ZnO and ZnO-Au samples were measured with Rhodamine B (RhB) as a dye pollutant under UV light (12 W). After the 10 mg of as-prepared photocatalyst dispersed in 20 mL of 5mg L^{-1} RhB aqueous solution, the target solution was magnetically stirred in the dark for 30 min to establish adsorption/desorption equilibrium between photocatalysts and RhB. Afterwards, the mixed solution was exposed to the UV light. At an interval of 30 min, 2 mL of the suspension was collected and centrifuged to remove the photocatalyst. The concentration of RhB was monitored by recording variations of the maximum absorbance at 553 nm using a Hitachi U-4100 spectrometer.

Results and Discussion

Figure 1 shows the XRD pattern of ZnO sample 1 prepared in a typical procedure by referring to the standard pattern of the ZnO powders from JCPDS files (JCPDS: 79-0205). The main diffraction peaks in Figure 1 can be assigned to the standard value of wurtzite structured ZnO (JCPDS no. 79–0205) with lattice parameters a= 3.241 Å and c = 5.187 Å. Moreover, the rest diffraction peaks at 12.2, 24.12, 33.2, and 44.3 ° (marked by circle in Figure 1) are indexed to crystalline TA, which can be found in pure TA reported in literature.[28] This confirms that the composition of the product contains TA, which is probably attributed to incomplete decomposition of TA. To evaluate the average crystallite sizes of ZnO from the strongest diffraction peaks, the Scherer equation was applied. The result indicates that the average crystallite size of the sample 1 is about 17.45 nm, which is larger than that of sample 2 prepared at 150 °C

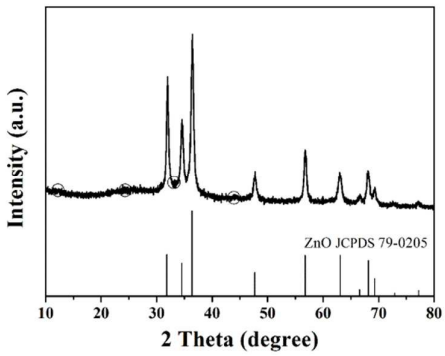

Figure 1 XRD pattern of sample 1 prepared at 100 °C for 6 h. The result revealed a typical wurtzite ZnO crystal structure (JCPDS no. 79–0205).

(15.70 nm, Figure S1b), indicating the reaction temperature improves the nucleation-growth rate of ZnO crystals.

To complement the XRD analysis and verify the existence of TA, the FTIR spectra of the precursor of sample 1, sample 1 and ZnO-700 were taken in a detection range of 400–4000 cm^{-1} as shown in Figure 2. To be more specific, a broad band at 3428 cm^{-1} is assigned to the O-H stretching mode of hydroxyl group and water molecules. And the FTIR peaks related to Zn–O bonds are clearly observed at 475, and 1385cm^{-1} in the spectra of b-c, which can be confirmed the formation of ZnO. Moreover, the FTIR spectra also confirms the existence of TA and the some organic residuals left after the TA decomposition based on the peaks of C-H (in the range of 2900 to 3000 cm^{-1}), C=O (1608 cm^{-1}), C-O (1049 cm^{-1}), and CO_3^{2-} (884 cm^{-1}). In contrast with the intensity of peaks in the precursor (Figure 2a), the intensity of peaks which belong to groups of TA in Figure 2b and c decreases with increasing the calcination temperature. It implies that TA was not decomposed completely when calcination temperature was below 700 °C which is higher than the decomposition temperature of pure TA.[28] It is probably attributed to the complex reaction among raw materials at low reaction temperature (100 °C), which prevent the TA from decomposing. Regrettably, we cannot find the composition of the precursor (Figure S1a). Above all, the obtained result indicates that the existence of TA in ZnO, which agrees well with the analysis of XRD.

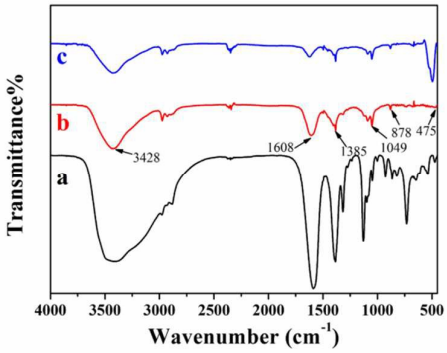

Figure 2 FT-IR spectrum of (a) the precursor of sample 1, (b) sample 1, and (c) ZnO-700.

Physical Chemistry Chemical Physics Accepted Manuscript

View Article Online
DOI: 10.1039/C5CP07187A

Published on 12 January 2016. Downloaded by Michigan State University on 20/01/2016 01:18:50.

In order to reveal the formation process of hierarchical butterfly-like ZnO in typical procedure, a series of experiments were carried out by varying reaction time. Figure 3 shows the SEM images of ZnO products obtained at 100 °C for 0, 3, 6, 9, and 12 h, respectively. At beginning, vast tiny NPs with a diameter of about 78.43 nm preferentially are formed, and it can be also seen the existence of few sheets in products (Figure 3a). By prolonging the reaction time to 3 h, the rudiment of butterfly-likeZnO was observed and it should be noting that some dispersed sheets still exist in the products (Figure 3b). At this stage, the morphology of the hierarchical ZnO has varied significantly. Large-scale butterfly-like ZnO products obtained under low reaction temperature (100 °C) is composed of ZnO sheets when the reaction time is prolonged to 6 h, as shown in the panoramic SEM image (Figure 3c). The hierarchical ZnO exhibits axial symmetry microstructure that is of a few micrometers in the range of 2.16-2.41 μm along the axial and 1.27-2.22 μm perpendicular to the axial. In particularly, the magnified SEM image in Figure 3d indicates the wings of butterfly-like ZnO with pore structure. With further increasing the reaction time to 9 h, the breadth and the length of butterfly-like microstructures increase to ~2.20 μm and ~5.10 μm, respectively (Figure 3e). With a longer reaction time of 12 h, the perfect butterfly-like products were obtained (Figure 3f). Experiment results suggest the growth of such butterfly-like ZnO involves an obvious nucleation-growth-assembly mechanism.

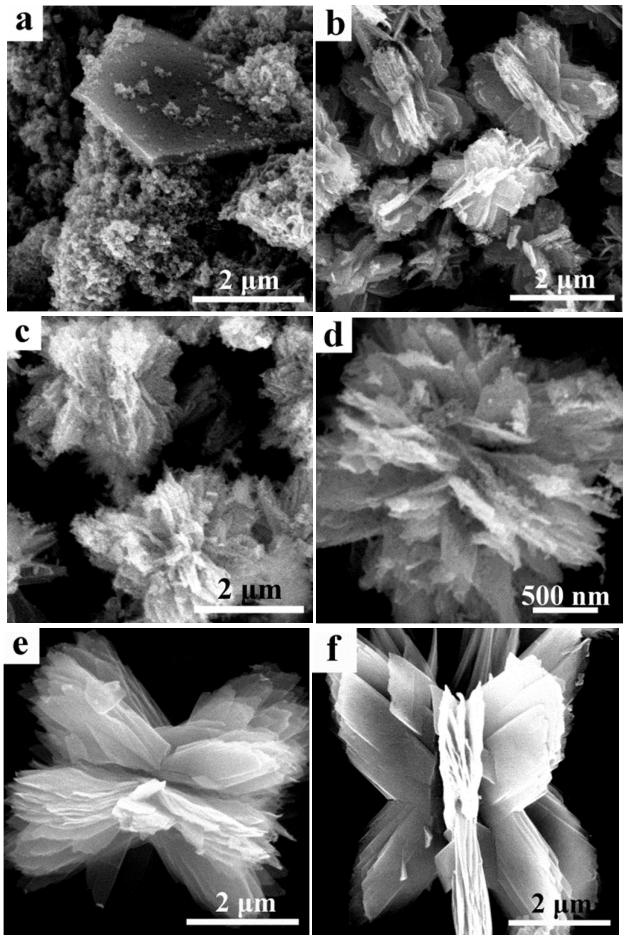

Figure 3 SEM images of ZnO samples synthesized at 100 °C for different reaction time: (a) 0 h, (b) 3 h, (c and d) 6 h (with different magnification), (e) 9 h, (f) 12 h.

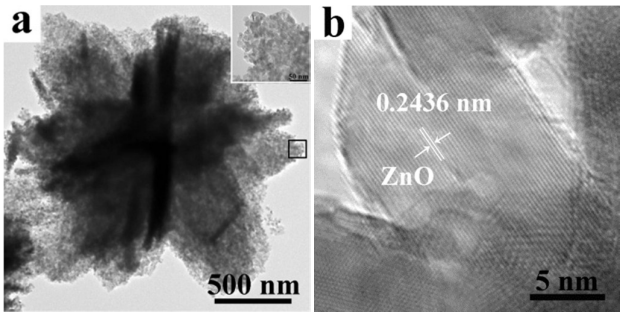

Figure 4 Low-magnification TEM image (a) of hierarchical butterfly-like ZnO (sample 1), and a HRTEM image (b) of the square region in part a.

The ZnO products obtained from a typical procedure were characterized using high-resolution transmission electron microscopy (HRTEM) for further structural analysis. The TEM images in Figure 4a and the inset manifest that sample 1 with butterfly-like microstructure. Moreover, sample 1 is composed of ZnO NPs with an average size of 16.67-18.0 nm, which is in accordance with the results obtained from Figure 1. The HRTEM image shown in Figure 4b recorded from square region in part a. The inter-planar spacing is a lattice of about 0.2436 nm, which is consistent with the crystal plane of (101) in ZnO. These results confirm that sample 1 is actually ZnO entity in our experiments.

To visually study the influence of reaction temperature on morphology of products, the SEM images of ZnO samples synthesized with different reaction temperature varying from 150 to 200 °C followed by calcination at 300 °C are shown in Figure 5. It was found that the morphologies of ZnO could be conveniently controlled by simply changing the reaction temperature. As the temperature increased to 150 °C from 100 °C, a large number of hierarchical flower-like ZnO appear, which are constituted by sharp petals with the length of 0.95~1.43 μm and the breadth of ~0.13 μm, respectively (Figure 5a). Further observation finds that a small fraction of dispersed ZnO plates generates in products, which is probably attributed to short reaction time of 6 h. When the reaction temperature is increased to 200 °C with other parameters kept constant, only a great number of irregular ZnO NPs are created as shown in Figure 5b. It indicates that reaction temperature has a great influence on the morphology of samples, which is consistent with the previous results.[29] The analysis of SEM images confirms that hierarchical ZnO microstructures are successfully fabricated at relatively low reaction temperature (100 -150 °C), however, irregular ZnO NPs can be obtained at high temperature (200 °C). The reason is that the reaction temperature could affect the nucleation and growth rate of crystals.[30]

To investigate the effect of the alkali concentration on the morphology of products, a series of samples were prepared.

Physical Chemistry Chemical Physics Accepted Manuscript

This journal is © The Royal Society of Chemistry 20xx

View Article Online
DOI: 10.1039/C5CP07187A

Published on 12 January 2016. Downloaded by Michigan State University on 20/01/2016 01:18:50.

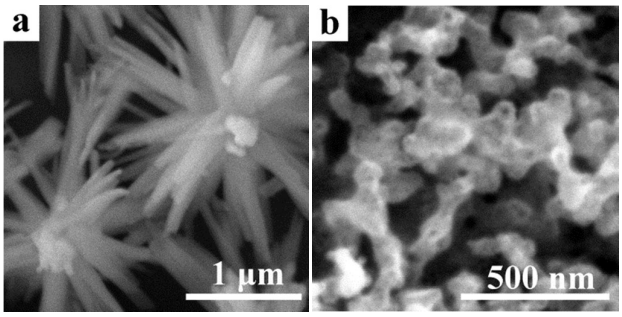

Figure 5 SEM images of samples synthesized at different reaction temperature: (a) sample 2, 150 °C; (b) sample 3, 200 °C.

The morphological analysis of as-prepared ZnO samples were carried out by SEM micrographs and depicted in Figure 6. The SEM images demonstrate the formation of different flower-like ZnO nanostructures. ZnO microspheres composed of microparticles were generated when the concentration of KOH was 0.10 M. The diameter of this sample ranged from 0.92 μm to 2.06 μm. However, small nanoparticles were still existed in the obtained products. By increasing the concentration to 0.15 M from 0.10 M, ZnO particles show peony shaped structures with a diameter of 1.27-1.59 μm. It is worth to mention that flower-like products with a few of petals were also emerged. By contrasting the morphology depicted in Figure 6 with that of sample 1, it is obvious that these ZnO products are relatively smaller than sample 1. This was attributed to that both the nucleation rate and crystal growth became relatively faster. In general, fast crystallization tended to form products with small dimension. In addition, clew-like microspheres are formed with different concentration of HMT (Figure S2). It needs to mention that there are a lot of irregular NPs observed in Figure S2. The possible reason is that HMT as a weak-base is not completely hydrolyzed at low temperature. Thus, high reaction temperature of 150 °C is employed to generate more hydroxyls by hydrolysis of HMT. As shown in Figure S3, clew-like ZnO microspheres consisted of sheets are generated when the concentration of HMT was ranged from 0.05 M to 0.15 M. It was found that the morphology of samples shown in Figure S2 and S3 greatly changed due to the effect of the weak base by comparison with others. From Figure S3, by increasing the concentration of HMT, ZnO microspheres with large size distribution obtained due to fast nucleation rate. The above analysis suggested the concentration of alkali and alkali source have a remarkable influence on morphology of ZnO products.

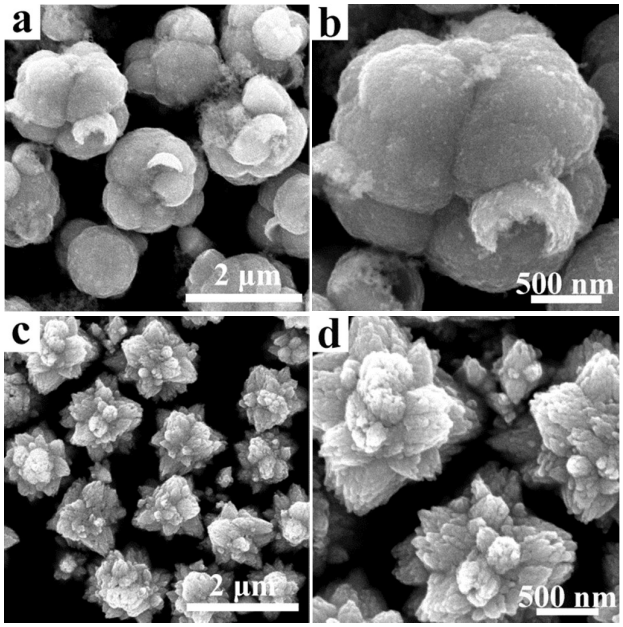

Figure 6 Typical SEM micrographs of samples synthesized with different concentrations of KOH: (a, b) sample 4, 0.10 M; (c, d) sample 5, 0.15 M.

ZnO-Au composite has attracted considerable attention as an efficient candidate for modifying ZnO to enhance photocatalytic activity. This is the first time to report hierarchical ZnO-Au successfully prepared by self-reducing ability of ZnO without any adscititious reductants in this paper. It was found that the color of ZnO aqueous solution was changed from initial white to purple rapidly upon adding $HAuCl_4 \cdot 3H_2O$ into the solution, indicating the formation of Au. To confirm this assumption, TEM and HRTEM measurements were performed on the as-obtained purple products and depicted in Figure 7. As shown in Figure 7a, it is worth noting that hierarchical butterfly-like ZnO-Au inherits the morphology of ZnO. Moreover, no Au NPs were found in this low-magnification TEM image, signifying the small size of Au NPs. Given to the higher magnification image of ZnO-Au in Figure 6b, it demonstrates that ZnO NPs are deposited with Au NPs where the dark spherical particles are ascribed to Au NPs and the light part is ZnO NPs. It is obvious that Au NPs with a diameter in the range of 3-7 nm are uniformly dispersed on the surface of ZnO NPs. In the HRTEM image (Figure 7c), ZnO and Au phases are clearly observed and closely contact to form an intimate interface. The lattice fringes of the (101) and (111) lattice planes have a spacing d of 0.2436 nm and 0.23 nm, agreeing well with the wurtzite ZnO and Au, respectively. Furthermore, EDS analysis of the ZnO-Au composite (sample 1-Au) also confirms the presence of Zn, O, and Au elements without any other elemental impurities, as shown in Figure 7d. According to the XRD pattern of sample 1-Au in Figure S1c, the diffraction peaks of Au do not appear because of the limited amount of Au NPs. The above-mentioned results can reveal that the synthesis of ZnO-Au by simple stirring at room temperature without any adscititious reductants is a masterly design. The self-reducing ability of butterfly-like ZnO was probably ascribe to the existence of residual TA in ZnO crystals calcined at 300 °C, in which they can be capable of reducing $HAuCl_4 \cdot 3H_2O$ on the surface of ZnO. The similar phenomenon was also discovered in aqueous solutions of sample 2a and 3, which can demonstrate the applicability of this method for preparing ZnO with self-reducing ability.

The To gain more insight into the chemical states of Zn and O in the butterfly-like ZnO, the sample were studied by using XPS analysis, and the corresponding results are shown in Figure 8. As observed in the high-resolution spectra for O

Physical Chemistry Chemical Physics Accepted Manuscript

View Article Online
DOI: 10.1039/C5CP07187A

Published on 12 January 2016. Downloaded by Michigan State University on 20/01/2016 01:18:50.

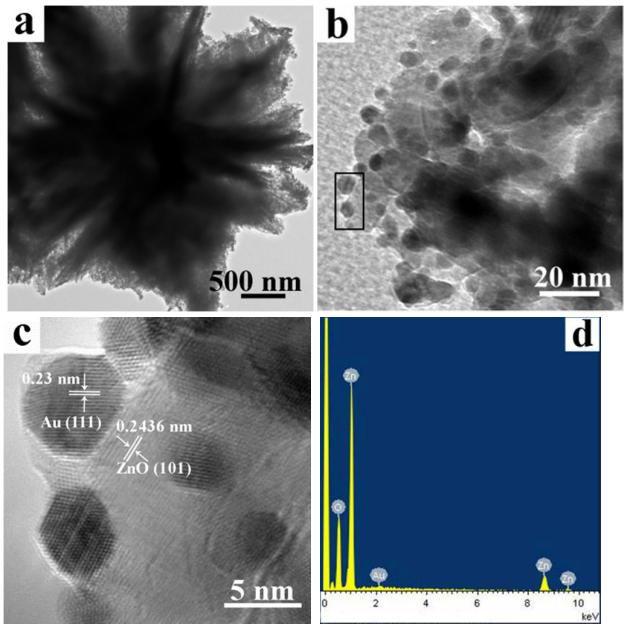

Figure 7 (a) Low-magnification TEM image of sample 1-Au; (b) TEM image, showing the formation of Au NPs; (c) HRTEM image of the rectangle region in part b; (d) EDS of sample 1-Au.

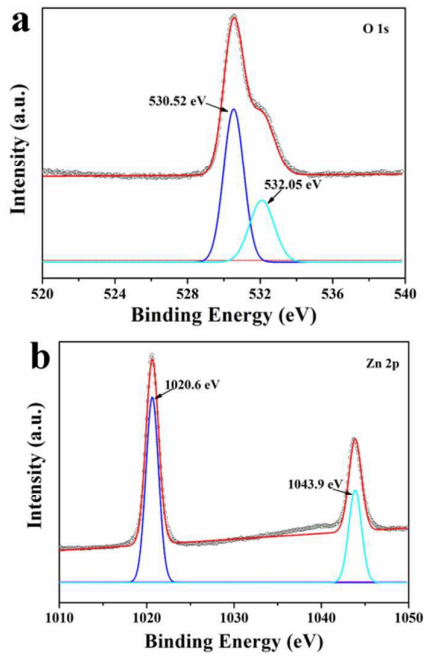

Figure 8 High-resolution XPS spectra of O 1s (a), and Zn 2p (b) in sample 1.

(Figure 8a), the shape of O_{1s} spectrum is asymmetric and can be described as the superposition of two peaks by Gaussian distribution, located around 530.52, and 532.05 eV, respectively, indicating two different kinds of O in this sample. The O_{1s} peak at low binding energy of 530.52 eV should be attributed to lattice oxygen in wurtzite structure of a hexagonal Zn^{2+} ion array.[31] This binding energy is close to the standard values of bulk ZnO. The O_{1s} peak located at 532.05eV is typically associated with loosely bound oxygen, such as hydroxyl groups or O_2^- ions in oxygen deficient regions. Furthermore, the calculated ratio of the adsorption oxygen to the lattice oxygen is 0.42, which is similar to the ratio reported in the previous literature.[32] As shown in Figure 8b, the symmetric Zn 2p peak can be observed, suggesting that there is one valence state of Zn in typical ZnO products. In addition, the binding energy of the Zn $2p_{3/2}$ and Zn $2p_{1/2}$ peaks in typical ZnO products are about 1020.6 eV and 1043.9 eV, respectively. Based on the above results, we can conclude that the zinc in the ZnO sample is in the Zn^{2+} valence state. Calculating with the peak areas, the relative ratios of lattice oxygen to zinc is about 1, indicating the formation of relatively perfect ZnO crystals.

Generally, there are two driving forces to assemble nanocrystals into nanosheets, namely anisotropic hydrophobic attraction and electrostatic interactions caused by dipole moments or surface charges. In our experimental, electrostatic interactions play the main role in governing the assembly process of NPs because no hydrophobic group provided in synthesis parameter. After the formation of sheets, the obtained sheets can experience the reconstruction process, which has been firstly reported by Shi and co-workers.[33] In this continuous reconstruction process, coarse sheets can be transformed into sheets with smooth surface, as shown in Fig. 3. Subsequently, a plausible process was proposed for the construction from sheets to 3D hierarchical ZnO. It can be considered as the assembly process derived from heterogeneous oriented attachments which are used to understand the behaviors of nucleation and growth.

According to the aforementioned results, a plausible mechanism of 3D hierarchical ZnO and ZnO-Au was speculated in Figure 9. The crystal-growth involves two mainly process, the formation of crystal nucleuses and secondly the growth and assembly of crystals. Initially, NPs were formed by the reactions among raw materials. Afterwards, the plans of these NPs gained not enough activation energy for nucleation and growth at low temperature. However, to achieve the minimum surface energy and to maintain the symmetry of the wurtzite crystal structure, followed by the assembled process of NPs toform 2D sheets, 3D symmetric butterfly-like products were synthesized by the assembly of sheets. In this period, TA could work as a morphology-controlling reagent via absorption on the surface of NPs. In our experiments, we found that the composition of precursors obtained by hydrothermal process

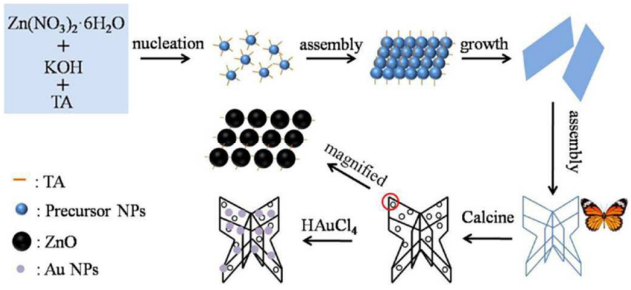

Figure 9 Schematic model of the formation of 3D hierarchical butterfly-like ZnO and ZnO-Au.

Physical Chemistry Chemical Physics Accepted Manuscript

This journal is © The Royal Society of Chemistry 20xx

View Article Online
DOI: 10.1039/C5CP07187A

Published on 12 January 2016. Downloaded by Michigan State University on 20/01/2016 01:18:50.

(at 100 °C for 6 h) was not clearly which was probably due to the synergistic effect of the excessive of $Zn(NO_3)_2{\cdot}6H_2O$ and the low reaction temperature. It should be noted that TA existed between NPs is not facile to remove by comparison with these TA on the surface of sheets. That is to say that TA in precursors is not completely decomposed, which result in the reduction of $HAuCl_4{\cdot}3H_2O$ without adscititious reductants due to the reducibility of hydroxyl in TA.

The optical properties of pure butterfly-like ZnO prepared by a typical procedure and the ZnO-Au composite were investigated by the analyses of DRS and PL spectra. DRS were used to study the influence of Au NPs on the light absorption of the pure ZnO. From Figure 10 a, the pure ZnO has strong light absorption in the wavelength range from 300 to 395 nm. Furthermore, a sharp edge at about 380 nm can be found in the spectrum of ZnO, which was related to the band gap of ZnO that is about 3.27 eV. For ZnO-Au sample, the characteristic surface plasmon band of Au NPs is observed at *ca.* 550 nm. Moreover, the absorption edges lightly moves to higher wavelength, revealing that ZnO-Au composite could be more efficient photocatalysts in photocatalysis field. Room-temperature PL measurements were widely used to investigate the properties of charge carrier separation and recombination properties. As shown in Figure 10b, PL spectra of sample 1 and sample 1-Au were obtained with an excitation wavelength of 325 nm. The two samples exhibit two similar peaks, where a narrow UV emission peak at about 390 nm corresponded precisely to near-band edge emission which can be assigned to the recombination of photo-generated electrons and holes,[34] whereas the broad emission peaks at around 476 nm belonged to an indirect emission which is initiated from interstitial-Zn-related defect.[35] Compared to the pure ZnO, the decrease of the UV emission peak indicated that the presence of Au promoted the separation and inhibited the recombination process of the photogenerated charge carriers.[36] In our case, that was because those Au NPs deposited on the surface of the ZnO would act as electron traps to capture the photo-generated electrons. The PL spectra proved the ZnO-Au composite was able to facilitate the electron-hole pair separation in comparison to the pure ZnO.

In order to investigate the electronic interaction between ZnO and Au NPs, the photocurrent transient response measurements for the butterfly-like ZnO and the ZnO-Au composite electrodes were carried out. As displayed in Figure11a, it was noticeable that the both electrodes showed fast and uniform photocurrent responses for every on−off cycle. Under UV light (365 nm) irradiation, it is clear that the measured photocurrent of the ZnO-Au electrode is higher than that of the pure ZnO electrode. As well know, the photocurrent was determined by the speed of photo-excited electrons withdrawn from ZnO-Au to ITO and the recombination at the electrode/electrolyte interface.[37] Hence, the enhanced photocurrent using ZnO-Au as the working electrode indicated the composite improved the separation rate of photogenerated electrons and holes. The photocatalytic performance of ZnO and ZnO-Au products under UV light irradiation were evaluated by monitoring the degradation of RhB in an aqueous solution. To compare the photocatalytic activity of different samples quantitatively, we detected the changes in RhB instantaneous concentration (C) relative to the initial concentration (C_0) during the photodegradation process. The photocatalytic efficiency of different samples was showed in Figure 11b and c, respectively. Prior to light illumination, the adsorption result obtained after 30 min dark treatment showed that the concentration of RhB was slight changed in Figure 11b and c. Under the UV illumination, the value of C/C_0 reduced in different degree with prolonging the time using different samples as the photocatalyst. For further analysis, the degradation efficiency of sample 1-Au reached about 99.9% after 90 min, whereas the lower value of about 56.19% was obtained after 180 min for pure ZnO sample. It can be attested to that the photocatalytic activity of ZnO in our experiment could be greatly improved after the deposition of Au NPs by comparison with the results reported by Peralta [18] and Sung [24]. Similarly, the degradation efficiency of sample 2 is of 37.27 % under the illumination of UV light for 3 h, which is drastically improved to 98.02% by introducing Au NPs onto ZnO (Figure 10c). Thus, the

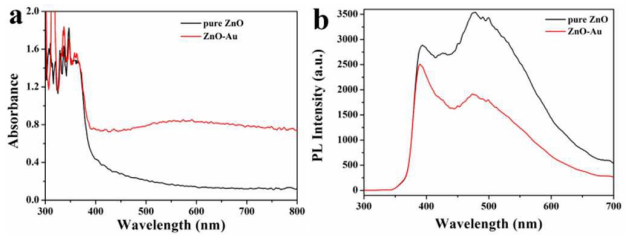

Figure 10 (a) UV−visible diffuse reflectance spectra and (b) room-temperature photoluminescence spectra of sample 1 and sample 1-Au.

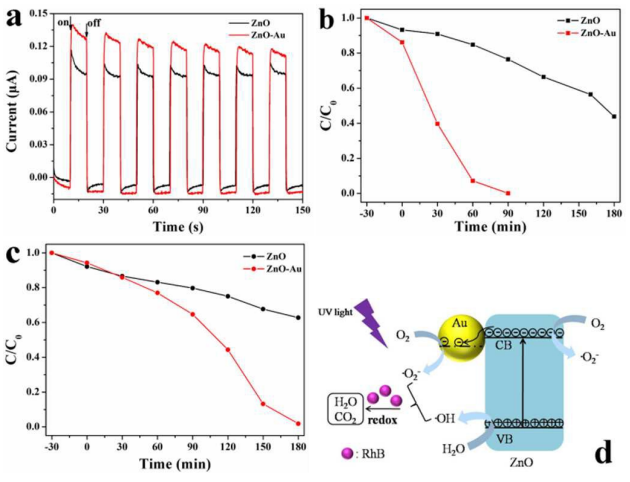

Figure 11 (a) Photocurrents and (b) photocatalytic degradation efficiency toward RhB of sample 1 and sample 1-Au under UV light irradiation. (c) Photodegradation of RhB using sample 2 and sample 2-Au under UV-light irradiation. (d) Enhanced photodegradation scheme of the ZnO-Au composite toward RhB.

Physical Chemistry Chemical Physics Accepted Manuscript

View Article Online
DOI: 10.1039/C5CP07187A

Published on 12 January 2016. Downloaded by Michigan State University on 20/01/2016 01:18:50.

results validate the practicability of the method investigated in this study. Furthermore, a photodegradation RhB dye mechanism of ZnO-Au composite is also proposed in Figure 11d. Under irradiation with UV light, electrons in valence band (VB) of ZnO getting enough energy can cross the band gap to CB, leaving behind holes in VB of semiconductors. Subsequently, Au NPs quickly absorb some electrons because a Schottky barrier is formed at the interface between ZnO and Au NPs. Au NPs acting as electron traps have a key role in inhibiting the recombination of photogenerated charge carriers and extending the lifetime of the electron–hole pairs. Then the excited electrons are trapped by the dissolve oxygen to yield $\cdot O_2^-$ radicals. Meanwhile, the holes in VB of ZnO are reacted with H_2O molecules to generate $\cdot OH$ radicals. Finally, owing to high activity of produced radicals, the dye molecules (RhB) can be destroyed into H_2O and CO_2 small molecules. Based on the above ananlysis, it clarified the availability of ZnO-Au in photocatalysis field synthesized in our experiments.

Conclusions

3D hierarchical ZnO microstructures with controllable morphologies were successfully prepared by a hydrothermal process followed by calcined treatment. It was found that the reaction temperature, alkali source, and the concentration of alkaline played a vital role for the morphology of the as-obtained ZnO samples. ZnO-Au composite was obtained by the reduction Au^{3+} to Au^0 in ZnO suspension without adding reducing agents. ZnO gained by calcination at 300 °C showed self-reducing ability which may be attributed to the existence of hydroxyl in residual TA. HRTEM revealed butterfly-like ZnO was composed of ZnO nanocrystals with a diameter of *ca.* 17.5 nm. Moreover, Au NPs were deposited uniformly on the surface of ZnO. Compared with pure ZnO, ZnO-Au composites exhibited appreciable photocatalytic activites toward RhB under UV light. The enhanced photodegradation was ascribed to that the introducing of Au NPs was in favor of promoting the separation process of the photo-generated e^-/h^+pairs.

Acknowledgements

This work was supported by the program for Taishan Scholars, the projects from National Natural Science Foundation of China (grant no. 51572109, 51501071, 51302106, 51402123, and 51402124).

Notes and references

1 G. k. Zhang, X. Shen and Y. Q. Yang, *J. Phys. Chem. C*, 2011, **115**, 7145.
2 A. Kubacka, M. Fernández-García and G. Colón, *Chem. Rev.*, 2012, **112**, 1555.
3 W. He, H. K. Kim, W. G. Wamer, D. Melka, J. H. Callahan and J. J. Yin, *J. Am. Chem. Soc.*, 2014, **136**, 750.
4 M. R. Alenezi, S. J. Henley, N. G. Emerson and S. R. P. Silva, *Nanoscale*, 2013, **6**, 235.
5 C. W. Sun, S. Rajasekhara, J. B. Goodenough and F. Zhou, *J. Am. Chem. Soc.*, 2011, **133**, 2132.
6 Y. Xiao, L. Lu, A. Zhang, Y. Zhang, L. Sun, L. Huo and F. Li, *ACS Appl. Mater. Interfaces*, 2012, **4**, 3797.
7 B. Li and Y. Wang, *J. Phys. Chem. C*, 2010,**114**,890.
8 D. E. Motaung, G. H. Mhlongo, S. S. Nkosi, G. F. Malgas, B. W. Mwakikunga, E. Coetsee, H. C. Swart, H. M. I. Abdallah, T. Moyo and S. S. Ray, *ACS Appl. Mater. Interfaces*, 2014, **6**, 8981.
9 E. W. Seelig, B. Tang, A. Yamilov, H. Cao and R. P. H. Chang, *Mater. Chem. Phys.*, 2003, **80**, 257.
10 H. M. Cheng and W. F. Hsieh, *Energy Environ. Sci.*, 2010, **3**, 442.
11 R. Shi, P. Yang, X. Dong, Q. Ma and A. Zhang, *Appl. Surf. Sci.*, 2013, **264**, 162.
12 Y. Shi, C. Zhu, L. Wang, C. Zhao, W. Li, K. K. Fung, T. Ma, A. Hagfeldt and N. Wang, *Chem. Mater.*, 2013, **25**, 1000.
13 B. Weng, M. Q. Yang, N. Zhang and Y. J. Xu, *J. Mater. Chem. A*, 2014, **2**, 9380.
14 P. Fageria, S. Gangopadhyay and S. Pande, *RSC Adv.*, 2014, **4**, 24962.
15 X. Wang, W. Liu, J. Liu, F. Wang, J. Kong, S. Qiu, C. He and L. Luan, *ACS Appl. Mater. Interfaces*, 2012, **4**, 817.
16 M. Raula, M. H. Rashid, T. K. Paira, E. Dinda and T. K. Mandal, *Langmuir*, 2010,**26**,8769.
17 Y. Yang, Y. Yang, H. Wu and S. Guo, *CrystEngComm*, 2013, **15**, 2608.
18 M. D. L. R. Peralta, U. Pal and R. S. Zeferino, *ACS Appl. Mater. Interfaces*, 2012, **4**, 4807.
19 S. W. Wang, Y. Yu, Y. H. Zuo, C. Z. Li, J. H. Yang and C.H. Lu, *Nanoscale*, 2012, **4**, 5895.
20 S. Balachandran and M. Swaminathan, *Dalton Trans.*, 2013, **42**, 5338.
21 Y. Wang, R. Shi, J. Lin and Y. Zhu, *Energy Environ. Sci.*, 2011, **4**, 2922.
22 P. Li, Z. Wei, T. Wu, Q. Peng and Y. Li, *J. Am. Chem. Soc.*,2011,**133**, 5660.
23 S. T. Kochuveedu, Y. H. Jang and D. H. Kim, *Chem. Soc. Rev.*, 2013, **42**, 8467.
24 Y. H. Sung, V. D. Frolov, S. M. Pimenov and J. J. Wu, *Phys. Chem. Chem. Phys.*, 2012, **14**, 14492.
25 J. Manna, T. P. Vinod, K. Flomin and R. Jelinek, *J. Colloid Interf. Sci.*, 2015, **460**, 113.
26 A. Morag, V. Ezersky, N. Froumin, D. Mogiliansky and R. Jelinek, *Chem. Commun.*, 2013, **49**, 8552.
27 A. Morag, N. Froumin, D. Mogiliansky, V. Ezersky, E. Beilis, S. Richter and R. Jelinek, *Adv. Funct. Mater.*, 2013, **23**, 5663.
28 D. Yalcin, O. Ozcalik, E. Altiok and O. Bayraktar, *J. Therm. Anal. Calorim.*, 2008,**94**, 767.
29 Z. Hong, M. Wei, T. Lan and G. Cao, *Nano Energy*, 2012,**1**, 466–471.
30 Y. Yang, Y. Yang, H. Wu and S. Guo, *CrystEngComm*, 2013, **15**, 2608.
31 W. Peng, S. Qu, G. Cong and Z. Wang, *Cryst. Growth Des.*, 2006, **6**,1518.
32 Y. Zheng, L. Zheng, Y. Zhan, X. Lin, Q. Zheng, and K. Wei, *Inorg. Chem.*, 2007, **46**, 6980.
33 Y. Shi, C. Zhu, L. Wang, C. Zhao, W. Li, K. K. Fung, T. Ma, A. Hagfeldt and N. Wang, *Chem. Mater.*, 2013, **25**, 1000.
34 X. H. Wang, D. X. Zhao, Y. C. Liu, J. Y. Zhang, Y. M. Lu and X. W. Fan, *J. Cryst. Growth*, 2004, **263**, 316.
35 H. Zeng, G. Duan, Y. Li, S. Yang, X. Xu and W. Cai, *Adv. Funct. Mater.*, 2010, **20**, 561.
36 R. Georgekutty, M. K. Seery and S. C. Pillai, *J. Phys. Chem. C*, 2008, **112**, 13563.
37 N. J. Bell, H. N. Yun, A. J. Du, H. Coster, S. C. Smith and R. Amal, *J. Phys. Chem. C*, 2011, **115**, 6004.

Physical Chemistry Chemical Physics Accepted Manuscript

This journal is © The Royal Society of Chemistry 20xx